Neuron
Article

Robo3-Driven Axon Midline Crossing Conditions Functional Maturation of a Large Commissural Synapse

Nicolas Michalski,[1,6] Norbert Babai,[1] Nicolas Renier,[2,3,4,7] David J. Perkel,[1,5] Alain Chédotal,[2,3,4] and Ralf Schneggenburger[1,*]
[1]Laboratory of Synaptic Mechanisms, Brain Mind Institute, School of Life Science, École Polytechnique Fédérale de Lausanne (EPFL), 1015 Lausanne, Switzerland
[2]INSERM, U968, Paris F-75012, France
[3]UPMC Univ Paris 06, UMR_S 968, Institut de la Vision, Paris F-75012, France
[4]CNRS, UMR_7210, Paris F-75012, France
[5]Department of Biology and Department of Otolaryngology, University of Washington, Seattle, WA 98195, USA
[6]Present address: Institut Pasteur, Unité de Génétique et Physiologie de l'Audition, Paris 75015, France
[7]Present address: Laboratory of Brain Development and Repair, The Rockefeller University, New York 10065, USA
*Correspondence: ralf.schneggenburger@epfl.ch
http://dx.doi.org/10.1016/j.neuron.2013.04.006

SUMMARY

During the formation of neuronal circuits, axon pathfinding decisions specify the location of synapses on the correct brain side and in correct target areas. We investigated a possible link between axon midline crossing and the subsequent development of output synapses formed by these axons. Conditional knockout of *Robo3* in the auditory system forced a large commissural synapse, the calyx of Held, to be exclusively formed on the wrong, ipsilateral side. Ipsilateral calyx of Held synapses showed strong transmission defects, with reduced and desynchronized transmitter release, fewer fast-releasable vesicles, and smaller and more variable presynaptic Ca^{2+} currents. Transmission defects were not observed in a downstream inhibitory synapse, and some defects persisted into adulthood. These results suggest that axon midline crossing conditions functional maturation of commissural synapses, thereby minimizing the impact of mislocalized synapses on information processing. This mechanism might be relevant to human disease caused by mutations in the ROBO3 gene.

INTRODUCTION

Neurons are arranged in ordered circuits which underlie information processing in the brain. The specificity of synaptic connections between partner neurons depends on pathfinding decisions during axon growth, which are mediated by axon guidance cues (Dickson, 2002). Upon the arrival of axons in their target area, there is an initial period of synaptogenesis, followed by a later, often experience-dependent period of synapse remodeling and synapse maturation, in which exuberant connections are pruned, and remaining connections acquire their specific synaptic strength and sets of synaptic plasticities (Sanes and Yamagata, 2009; Shen and Scheiffele, 2010). Therefore, axon pathfinding decisions, followed by later programs of synaptogenesis and synapse maturation, ensure the specificity of synaptic wiring in the brain.

Synaptic connections in the CNS greatly vary in terms of their transmission strength (Sherman and Guillery, 1998; Walmsley et al., 1998). It might be expected that synapses formed by axons that contact neurons in distant, and often contralateral target areas, should have a strong influence on the action potential (AP) firing of their postsynaptic neurons ("driver" or "relay" type of synapses; Sherman and Guillery, 1998). Genetic ablation of axon guidance proteins or of their receptors has been shown to lead to aberrant wiring of axons, particularly at the midline (Brose et al., 1999; Fazeli et al., 1997; Kidd et al., 1999; Serafini et al., 1996; for review see Chédotal, 2011). However, it has remained relatively unexplored whether misguided axons can form functionally normal synapses. It could be expected that feedback mechanisms exist that suppress the function of synapses formed in inappropriate target areas, or on the wrong side of the brain, but the existence of such mechanisms is largely unknown.

The calyx of Held synapse in the mammalian central auditory system is an ideal model to address this question. The calyx of Held projection is a major commissural afferent pathway of the auditory brainstem, formed by axons of globular bushy cells (GBCs) in the ventral cochlear nucleus (VCN), that synapse onto principal neurons of the medial nucleus of the trapezoid body (MNTB; Cant and Benson, 2003; Figure 1A). In wild-type mice, more than 99% of all calyces originate from the contralateral VCN (Hsieh et al., 2007), highlighting the importance of axon midline crossing for this connection. Following axon midline crossing at around E14 in mice (Howell et al., 2007), bouton-like synapses are established between VCN and MNTB neurons in a period of initial synaptogenesis around birth. The monoinnervation of an MNTB neuron by a single large calyx of Held is only established between postnatal days 2 (P2) and P5, in a nerve

terminal growth program that includes calyx growth, and the elimination of competing synaptic inputs (Hoffpauir et al., 2006; Hoffpauir et al., 2010; Rodríguez-Contreras et al., 2008). From P5 onward and extending beyond the onset of hearing (which occurs at P12 in mice; Ehret, 1976), further processes of synapse maturation enable the calyx to acquire its characteristic fast transmitter release properties. These developmental changes include a speeding of presynaptic AP width, changes of presynaptic Ca^{2+} channel subtypes, and tighter Ca^{2+} channel-vesicle colocalization (Fedchyshyn and Wang, 2005; Iwasaki et al., 2000; Taschenberger and von Gersdorff, 2000).

MNTB neurons make inhibitory output synapses onto neurons of the lateral superior olive (LSO; Kim and Kandler, 2003) and on other output nuclei ipsilateral to the MNTB. Therefore, the function of the large calyx of Held is that of a rapid excitatory relay synapse, which converts an AP arising from a GBC into fast inhibition of neurons on the contralateral auditory brainstem, including LSO (Figure 1A; see Borst and Soria van Hoeve, 2012 for review). LSO neurons then compare direct ipsilateral excitation with inhibition arising from the contralateral ear, to compute sound source localization based on interaural sound intensity differences (Grothe et al., 2010). In this circuit, failure of midline crossing by the calyx of Held axons is expected to seriously distort this computation, because the inhibition provided by MNTB neurons would now converge onto excitation arising from the same side of the brain (Figure 1A).

Robo3 is one of a family of Robo proteins (Roundabout) which are transmembrane receptors of the immunoglobulin superfamily (Ypsilanti et al., 2010). Robo1 and Robo2 are receptors for the midline repellent guidance cues Slits (Brose et al., 1999; Kidd et al., 1999); the mechanism of Robo3 action is currently debated (Ypsilanti et al., 2010). Inactivation of the *Robo3* gene in conventional knock-out mice has revealed an absolute requirement of Robo3 for commissural axon midline crossing in the spinal cord and hindbrain (Marillat et al., 2004; Sabatier et al., 2004). Here, we used *Robo3* conditional knockout mice (Renier et al., 2010), to investigate whether misguided commissural axons can elaborate morphologically and functionally normal synapses. In these mice, we found a strong deficit of presynaptic function of ipsilateral calyx of Held synapses that persisted beyond hearing onset. Our results suggest that midline crossing decisions made by axons at early developmental ages condition the maturation of synapse function later on.

RESULTS

Anatomical Organization of the Calyx of Held Projection in Robo3 cKO Mice

Midline crossing of commissural axons in the mammalian hindbrain critically depends on Robo3 (Renier et al., 2010). Here, we used the *Robo3* floxed allele (Renier et al., 2010), and the *Krox20::Cre* mice (Voiculescu et al., 2000), to conditionally inactivate *Robo3* in the lower auditory brainstem, including neurons of the VCN (Farago et al., 2006; Han et al., 2011; Maricich et al., 2009). This allowed us to study the development of calyces formed on the wrong, ipsilateral side of the brain.

We first used bilateral VCN injection of two lipophilic tracers (DiI and DiA), to anatomically investigate the axon midline crossing deficit in $Krox20^{Cre/+}$, $Robo3^{lox/lox}$ mice (which will be referred to as Robo3 cKO mice). We used Cre-negative $Krox20^{+/+}$, $Robo3^{lox/lox}$ littermate mice as control mice (see Experimental Procedures). The dual-color labeling of axons demonstrated that in control mice, projections to each MNTB originated selectively from the contralateral VCN. In contrast, in Robo3 cKO mice, there was a clear absence of crossing axons, and projections to the MNTB originated ipsilaterally (Figure 1B). We next performed immunohistochemistry with anti-parvalbumin (PV) and anti-synaptotagmin 2 (Syt2) antibodies, to label calyceal axons and nerve terminals, or calyceal nerve terminals alone, respectively. Numerous PV-positive axons could be seen at the midline of a P5 control mouse (Figure 1C, top), whereas midline-crossing axons were essentially absent in Robo3 cKO mice (Figure 1C, bottom). In addition, these images showed that in Robo3 cKO mice, fibers entered the MNTB from the lateral side (Figure 1C, arrow). The absence of midline-crossing axons in Robo3 cKO mice was consistently observed throughout the anterior-posterior axis of the MNTB, and was also observed in an adult (P58) Robo3 cKO mouse (data not shown). Therefore, essentially all calyx of Held—generating axons target the wrong, ipsilateral side of the brain in Robo3 cKO mice.

Auditory brainstem neurons are aligned in a tonotopically organized manner according to their characteristic sound frequency. In the MNTB, this tonotopic gradient runs along the mediolateral axis, and a tonotopic gradient is also found in the VCN and in other auditory nuclei (Friauf, 1992). This suggests that VCN axons contact specific postsynaptic neurons within the MNTB, according to their positions along the tonotopic axis. To test whether the tonotopic targeting of postsynaptic neurons was affected in Robo3 cKO mice, we labeled neurons with high characteristic sound frequencies, using the c-fos labeling technique and a 35 kHz pure tone exposure (Friauf, 1992; Miko et al., 2007). In P20 control mice, labeled MNTB neurons were found in the most medial third of the nucleus (Figure 1D, left; Friauf, 1992; Miko et al., 2007). In Robo-3 cKO mice, the mapping pattern was not markedly changed, since labeled neurons were also found in the most medial third of the MNTB (Figure 1D, right). Remarkably, this suggests that VCN axons reached their correct target neurons with respect to the mediolateral axis in Robo3 cKO mice, even though the axons had a complete midline crossing defect.

Multiple Innervation and Strong Deficit of Synaptic Transmission at the Calyx of Held Synapse in Robo3 cKO Mice

To probe the function of ipsilateral calyces of Held in Robo3cKO mice, we recorded EPSCs in MNTB neurons following afferent fiber stimulation, initially using P9–P12 old mice (Figure 2). The stimulation electrode was placed on the medial side of the MNTB in control animals (Figure 2A) and on the lateral side of the MNTB in Robo3 cKO mice (Figures 2B and 2C), in agreement with our anatomical results (see above). Recordings in control mice showed large and fast EPSCs with a sharp threshold, indicating that a single presynaptic fiber caused the EPSCs (Figures 2A and 2E; Bergsman et al., 2004; Hoffpauir et al., 2006). In

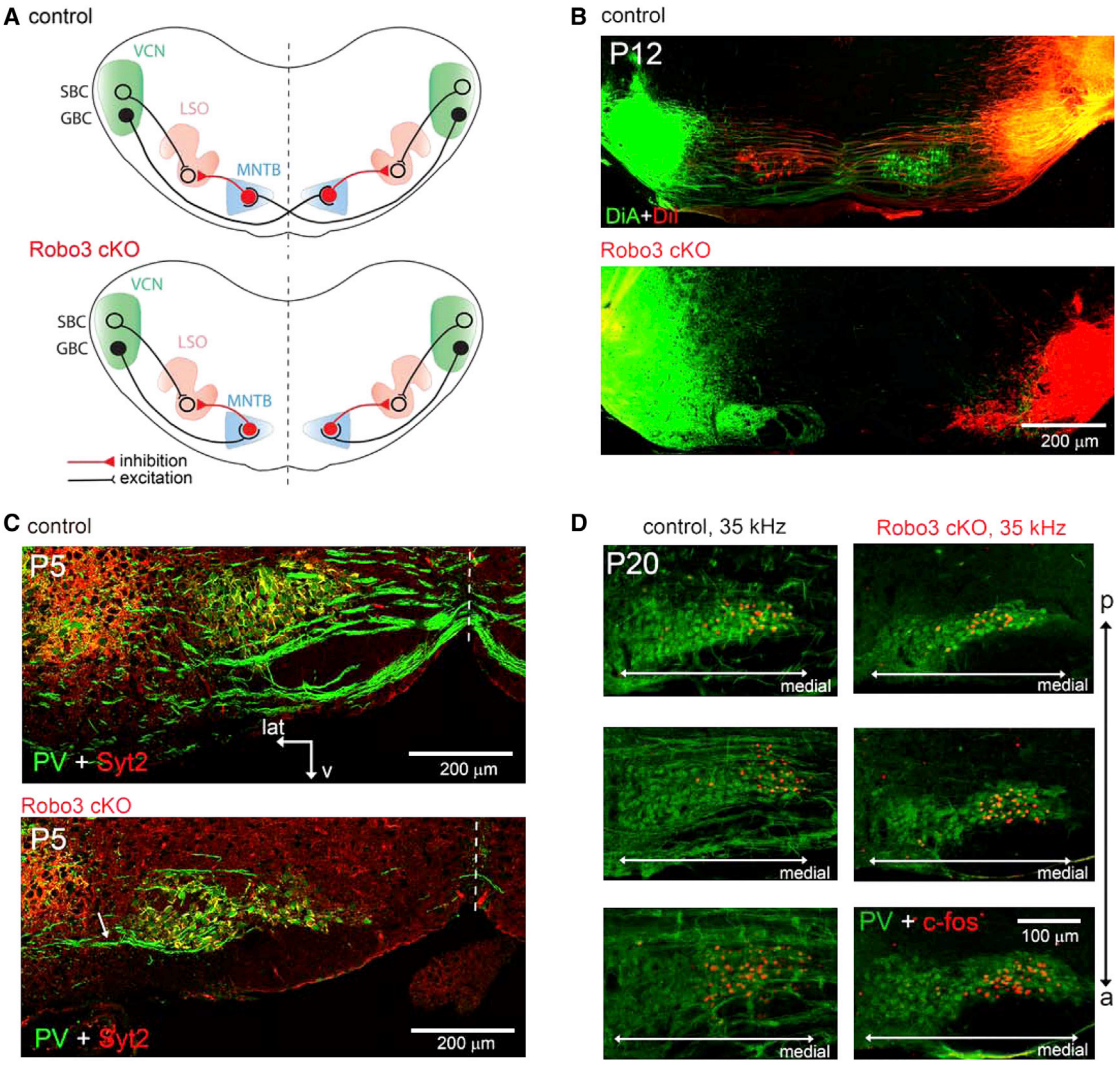

Figure 1. Anatomical Organization of the VCN to MNTB Projection in Robo3 cKO Mice

(A) Scheme of the auditory brainstem circuit showing ventral cochlear nucleus (VCN) with spherical and globular bushy cells (SBC and GBC, respectively), the lateral superior olive (LSO), and medial nucleus of the trapezoid body (MNTB). Note that unilateral sound exposure normally leads to inhibition of the contralateral LSO via the crossed calyx of Held projection. In the absence of midline crossing of the GBC axons, inhibition is expected to erroneously take place in the ipsilateral LSO.

(B) Transverse sections of P12 control and Robo3 cKO mice injected with either DiI or DiA in each cochlear nucleus. This double-color staining clearly demonstrates the contralateral origin of the VCN axons that form the calyx of Held synapses in the control mouse (top), whereas in the Robo3 cKO mouse, the projection originates ipsilaterally. The ventral orientation points downward.

(C) Immunohistochemistry of the superior olivary complex in a Robo3 cKO mouse and a control littermate mouse at P5, with anti-Syt2 and anti-PV antibodies. Note the almost complete absence of PV-immunoreactive axons at the midline, and PV-immunoreactive fibers entering the MNTB from the lateral side (arrow) in the Robo3 cKO mouse. In this and all images in subsequent figures, ventral (v) points downward, and lateral (lat) points to the left.

(D) Activity-dependent labeling of neurons with a high characteristic sound frequency in the MNTB. Robo3 cKO and control mice at age P20 were exposed to a 35 kHz pure tone, and immunohistochemistry was performed using anti-PV and anti- c-*fos* antibodies. For each animal, three sections aligned in the posterior to anterior extension (p-a) are shown. The estimated mediolateral extension of the MNTB is indicated by the white arrow. Note that in Robo3 cKO mice, high characteristic sound frequency neurons are located close to the medial pole of the MNTB, similarly as in control mice.

contrast, much smaller EPSCs were observed in most Robo3 cKO neurons, and increasing the stimulus intensity revealed several (up to three) synaptic inputs, each with small amplitudes (Figure 2B). We occasionally observed MNTB neurons with single large EPSCs in Robo3 cKO mice (Figure 2C). Across all cells, however, the average maximal EPSC amplitude was significantly smaller in Robo3 cKO mice (2.88 ± 0.76 nA, n = 22 cells) as compared to control mice (9.42 ± 1.94 nA, n = 9 cells; $p < 0.01$) (Figure 2D). Thus, there was a strong functional deficit of synaptic transmission in these mice.

We found that the majority of the neurons in the Robo3 cKO mice showed more than one synaptic input, whereas most

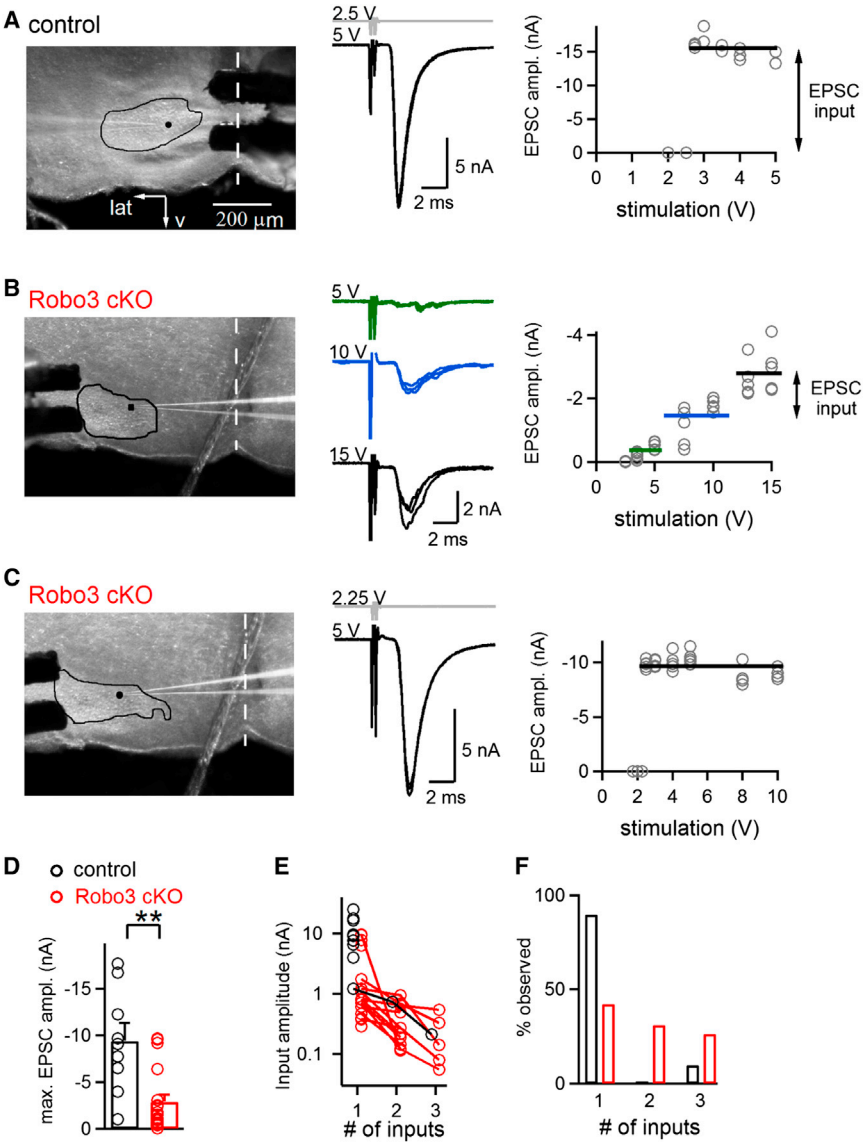

Figure 2. Fiber Stimulation Experiments Reveal Impaired Synaptic Transmission at the Calyx of Held of Robo3 cKO Mice

(A–C) Panels show images of the position of stimulation electrodes and recording pipettes (left), example EPSC traces at different stimulation intensities (middle), and plots of EPSC amplitude as a function of stimulation voltage (right) in P9–P12 mice. The data in (A) is from a control mouse, whereas the data in (B) and (C) are from two different Robo3 cKO mice. In the images, the extension of the MNTB nucleus and the recording sites are indicated by black lines, and black dots, respectively.

(D–F) Average maximal EPSC amplitudes (D), amplitudes of individual EPSC inputs (E) and histograms of the number of detected synaptic inputs (F), are shown for both control and Robo3 cKO mice (black, and red symbols respectively). In this and all subsequent figures, red and black symbols refer to data from Robo3 cKO synapses and control synapses, respectively.

The error bars represent SEM.

neurons in control mice had single-fiber-mediated EPSCs (Figures 2E and 2F; red and black symbols, respectively). This suggests that in Robo3 cKO mice, MNTB neurons receive a significantly larger number of synaptic inputs, indicating a deficit in synapse elimination in addition to the smaller absolute EPSC amplitudes.

The Synaptic Transmission Deficit Has a Presynaptic Origin

To determine whether the decreased EPSC amplitude was caused by pre- or postsynaptic defects, we next investigated the kinetics of fiber stimulation-evoked EPSCs, their paired-pulse ratio (EPSC2/EPSC1), and the amplitude and frequency of miniature (quantal) EPSCs (mEPSCs; Figures 3A–3D). In Robo3 cKO mice, the evoked EPSCs had significantly longer rise times, irregularities during the rise and decay phases, and a significantly increased paired pulse ratio (Figures 3A and 3B). The amplitude and frequency of mEPSCs were unchanged in Robo3 cKO mice, and similarly, the mEPSC decay time constant was unchanged (Figures 3C and 3D; $p > 0.05$). These findings suggest that a reduced transmitter release is the cause for the reduced EPSC amplitude in Robo3 cKO mice, without obvious postsynaptic deficits.

Since evoked EPSCs showed signs of desynchronized release in Robo3 cKO mice (Figure 3A), reminiscent of EPSCs in younger animals (Chuhma et al., 2001), we searched for other signs of immaturity at the calyx of Held synapse in Robo3 cKO mice. Calyx of Held synapses show a presynaptic form of plasticity, posttetanic potentiation (PTP), which is easily induced in immature synapses, but requires stronger induction stimuli in more mature synapses (Habets and Borst, 2005; Korogod et al., 2005). We therefore measured PTP in Robo3 cKO mice, to independently assess the maturation state of calyx synapses. In control mice at P9–P12, we found moderate PTP to 140% ± 30% of the control EPSC amplitude (n = 3; Figure 3E). In Robo3 cKO mice at the same age, PTP was dramatically increased (Figure 3F; 460% ± 50%; n = 3; $p < 0.01$). PTP was also increased in P18–P22 Robo3 cKO mice (320% ± 10%, n = 4) as compared to control mice of the same age (130% ± 40%; n = 3), although this difference did not reach significance ($p = 0.12$). Together, the findings of desynchronized transmitter release, and of increased PTP suggest that calyx of Held synapses have more immature transmitter release properties in Robo3 cKO mice as compared to control mice.

The measurements of fiber stimulation-evoked EPSCs suggested that MNTB neurons are innervated by multiple synaptic

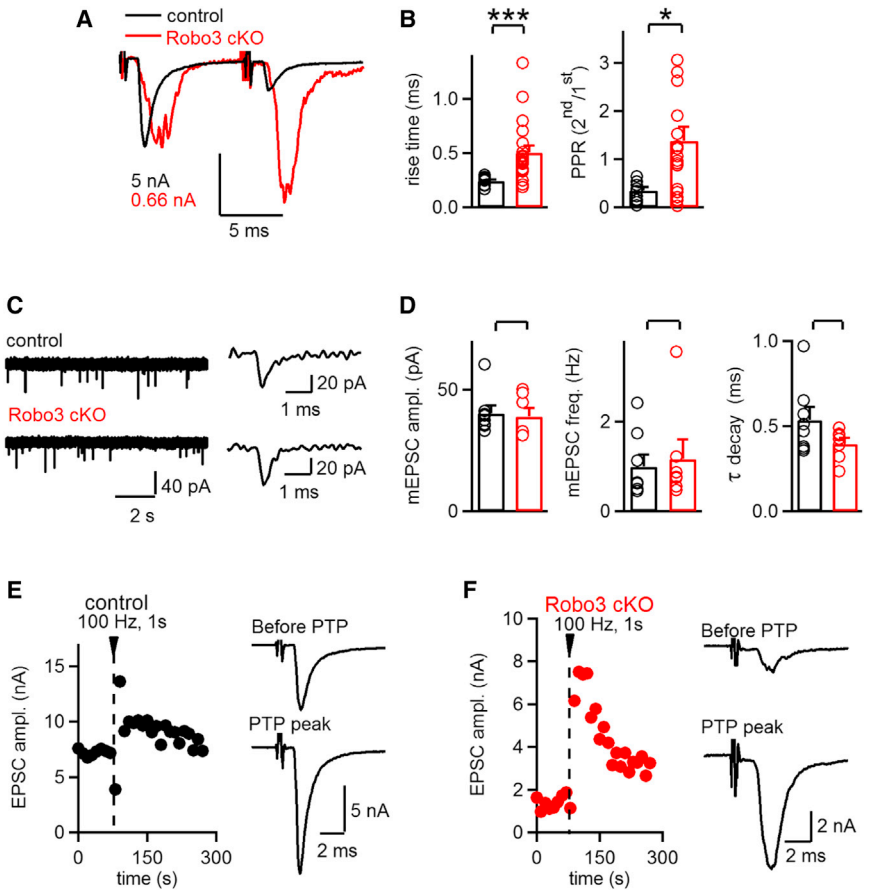

Figure 3. Presynaptic Deficits and Severe Signs of Immaturity at the Calyx of Held Synapse of Robo3 cKO Mice

(A) Overlay of EPSC traces in response to paired stimuli in a control mouse (black trace), and in a Robo3 cKO mouse (red trace; peak-scaled to the first EPSC in the control mouse).

(B) Quantifications of the EPSC rise time (left) and of the paired-pulse ratio (PPR; right). These values are significantly different between Robo3 cKO mice (red symbols) and control mice (black symbols). Note that one clear outlier data point was removed (PPR of 1.85 in a control recording).

(C) Example traces of mEPSC recordings in a control mouse (top) and in a Robo3 cKO mouse (bottom).

(D) Average values of the mEPSC amplitude (left), mEPSC frequency (middle), and mEPSC decay time constant (right). The values of these parameters are not significantly different between Robo3 cKO (red symbols) and control mice (black symbols).

(E and F) Posttetanic potentiation (PTP) in response to 1 s 100 Hz trains of afferent fiber stimuli in a control mouse (E), and in a Robo3 cKO mouse (F). Example traces for the corresponding recording before, and following the high frequency train are also shown.

All recordings presented were obtained from P9- to P12-old mice. The error bars represent SEM.

terminals in Robo3 cKO mice (see above; Figure 2). To confirm multiple innervation anatomically, we filled single calyces of Held with Alexa 488 in presynaptic patch-clamp recordings. In post hoc immunohistochemistry, we then visualized all calyx-type nerve terminals in close apposition to the postsynaptic neuron, using anti-Syt2 and anti-PV antibodies as calyceal markers (Figure 4A). As expected, Syt2-immunoreactive nerve terminals not filled by Alexa 488 (and larger than ~2 μm^2) could hardly be detected in control mice (Figure 4A, top). In contrast, in Robo3 cKO mice, relatively large, secondary Syt2- and PV-immunoreactive nerve terminals not filled by Alexa 488 were frequently observed (see Figure 4A, bottom, for an example). We used three-dimensional (3D) rendering to measure the surface area of the largest nonfilled Syt2-immunoreactive nerve terminals. This value was small in control mice (1.87 ± 1.5 μm^2; n = 8) but much larger in Robo3cKO mice (23.2 ± 8.6 μm^2; n = 9, $p < 0.05$) (Figure 4B). This provides clear anatomical evidence for multiple innervation of MNTB neurons in Robo3 cKO mice.

We next measured the surface area of the dye-filled, primary calyx nerve terminals following three-dimensional rendering (Figures 4A and 4C; green channel). We found that the calyx surface was reduced by about 35% in Robo3 cKO mice as compared to control mice (Figure 4C; $p < 0.01$). The smaller membrane surface of the largest, primary calyx terminal might be a consequence of the synapse elimination deficit and the continued presence of secondary nerve terminals, which likely compete for space with the largest calyx (Figure 4A, right). In conclusion, dye-filling experiments in combination with post-hoc immunohistochemistry provide independent evidence for a synapse elimination deficit at the calyx of Held synapse of Robo3 cKO mice.

Smaller Presynaptic Ca^{2+} Current and Fewer Fast-Releasable Vesicles in Robo3 cKO Mice

To investigate the presynaptic defects underlying the impaired synaptic transmission, we performed simultaneous pre- and postsynaptic recordings (Figure 5). The presynaptic Ca^{2+} currents in response to a 50 ms depolarization to 0 mV were significantly smaller in Robo3 cKO mice (0.82 ± 0.10 nA; n = 26) as compared to control mice (1.40 ± 0.10 nA, n = 14; $p < 0.001$) (Figures 5A and 5B). The basal presynaptic membrane capacitance (C_m), a proxy of the membrane surface of the calyx, was smaller in Robo3 cKO mice (15.4 ± 1.4 pF) than in control (22.4 ± 1.4 pF; $p < 0.001$; Figure 5B). This agrees well with the smaller calyx surface found in the three-dimensionally rendered calyces (Figure 4C). The Ca^{2+} current density, calculated by normalizing the maximal Ca^{2+} current by the C_m value of each recording, was unchanged on average ($p = 0.35$), but was more variable in Robo3 cKO mice (Figure 5B).

The EPSCs in response to pool-depleting presynaptic depolarizations were smaller and had slower rise times in Robo3 cKO mice (Figure 5A), indicating smaller pool sizes and less synchronized transmitter release. Deconvolution analysis of EPSCs

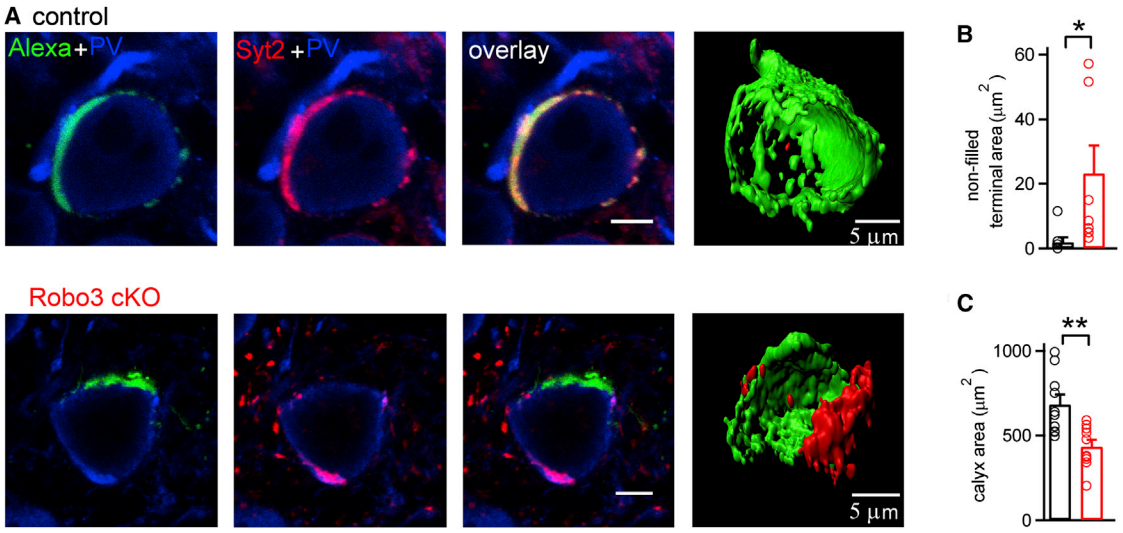

Figure 4. Smaller Calyx Size and Multiple Innervation in Robo3 cKO Mice

(A) Example images of calyces filled with Alexa 488 (green channel) via the patch-pipette and costained by immunohistochemistry with anti-Syt2 (red) and anti-PV antibodies (blue channel), both for a control mouse (top) and for a Robo3 cKO mouse (bottom). The rightmost images represent three-dimensional reconstructions using the Alexa-488 channel (green), and the Syt2 channel (red). Note that while in the control mouse, the anti-Syt2 stain and the Alexa fill largely overlap, in the Robo3 cKO mouse, there was a prominent Syt2-immunoreactive nerve terminal which was not filled via the patch-pipette, indicating innervation with a second calyx-like nerve terminal.

(B and C) Quantifications of the surface area of the largest non-filled Syt2-positive nerve terminal (B), and of the Alexa 488 filled primary calyx nerve terminal (C). Note the significantly larger size of secondary nerve terminals (B), and the significantly smaller calyx size (C) in Robo3 cKO mice (red symbols) as compared to control mice (black symbols).

All data in this figure were obtained from P9–P12 old mice. The error bars represent SEM.

indeed showed a strong reduction of the fast release component in Robo3 cKO mice. In the example of a Robo3 cKO recording in Figure 5A3, release was very slow and the cumulative release trace could be fitted with a single exponential with a time constant of 26 ms. Overall, n = 8 out of 20 synapses recorded in Robo3 cKO mice showed similarly slow release, with time constants of 10 ms or more. Over the entire population of synapses, the release time constant was significantly slower in Robo3cKO as compared to control mice (Figure 5C). Furthermore, the number of vesicles released in the fast component was significantly lower in Robo3 cKO mice (772 ± 98; n = 12 cells) as compared to control calyces (1,602 ± 196; n = 10; $p < 0.001$) (Figure 5C). Thus, the vesicle release kinetics were slowed, and there were fewer vesicles in the fast-releasable subpool, FRP (Sakaba and Neher, 2001).

Previous work has shown that phasic transmitter release in response to presynaptic APs is mainly contributed by FRP vesicles (Sakaba, 2006). Therefore, we would expect that a lower number of FRP vesicles in Robo3 cKO mice should translate into a similar decrease in the number of fast-releasable vesicles available for AP-evoked release. To test this prediction, and to investigate possible changes in release probability, we used 100 Hz trains of brief AP-like presynaptic depolarizations, and back-extrapolation of cumulative EPSC amplitudes as a pool size estimate (Schneggenburger et al., 1999; Figures 5D and 5E). The EPSCs evoked by brief AP-like depolarizations were significantly smaller, and 100 Hz trains caused significantly larger initial facilitation in Robo3 cKO than in control mice (Figure 5D2). The method of cumulative EPSC amplitudes (Figure 5E) revealed a significantly smaller pool size in Robo3 cKO mice (8.6 ± 3.5 nA; n = 5) as compared to control mice (25.7 ± 4.8 nA; n = 7; $p = 0.012$). Furthermore, there was a significant reduction of release probability during the first EPSC, as estimated by dividing the first EPSC amplitude by the pool size estimate (Figures 5E1 and 5E2).

In summary, direct pre- and postsynaptic recordings at ipsilateral calyx of Held synapses indicate a more variable Ca^{2+} current density, a smaller size of the fast-releasable vesicle pool (FRP), and a significant reduction of the initial release probability in Robo3 cKO mice (Figure 5). These data show that processes of synapse maturation, including the acquisition of fast transmitter release properties characteristic for the calyx of Held, fail to take place in Robo3 cKO mice.

Postnatal Inactivation of *Robo3* Does Not Affect Synaptic Transmission at Calyx of Held Synapses

The finding of functional deficits at the calyx of Held synapses in Robo3 cKO mice suggests that axon midline crossing conditions the functional maturation of commissural output synapses. Alternatively, Robo3 could have a so far unknown direct role in synapse formation and synapse maturation. In a first series of experiments, we addressed this possibility by studying the developmental expression of Robo3, to verify whether Robo3 is expressed at the time of synaptogenesis (Figures 6A–6C). In situ hybridization showed Robo3 expression at E14 in the developing VCN, but transcript levels in the VCN were essentially absent at E18 and undetectable at P10 (Figure 6A). Using an anti-human Robo3 antibody which stained crossing hindbrain

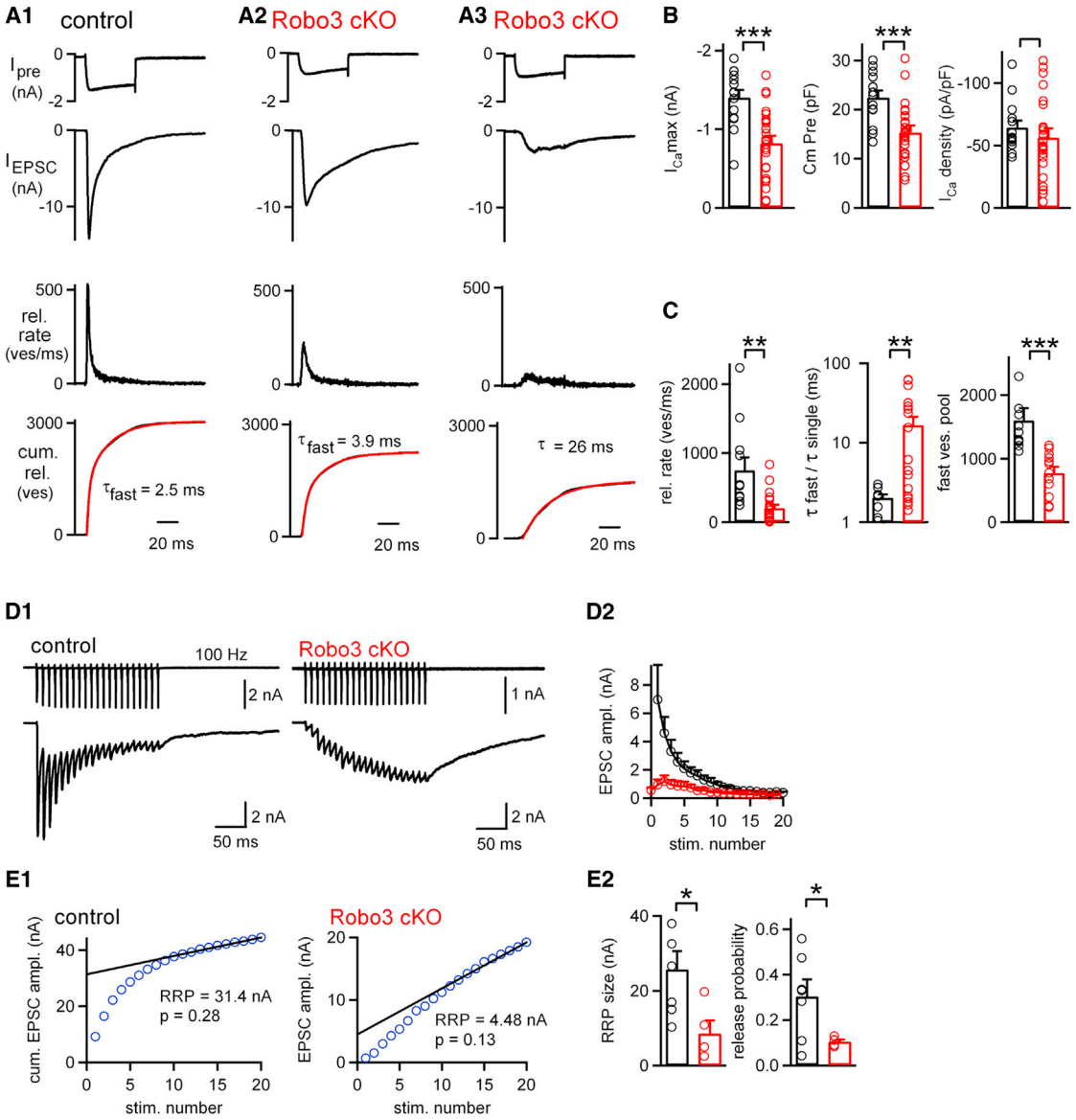

Figure 5. A Reduction of the Fast-Releasable Vesicle Pool FRP, and More Variable Presynaptic Ca^{2+} Currents Explain the Transmission Deficit in Robo3 cKO Mice

(A1–A3) Transmitter release in response to prolonged 50 ms presynaptic depolarizations to 0 mV in a paired recording in a control mouse (A1), and for two example recordings in Robo3 cKO mice (A2, and A3). The individual panels from top to bottom show presynaptic voltage-gated Ca^{2+} currents, EPSCs, release rates as revealed by EPSC deconvolution (Neher and Sakaba, 2001) and traces of cumulative release. The cumulative release traces are overlaid with the best exponential fit functions (red line; double-exponential in A1, A2, and single exponential in A3). Note the strong slowing, or even absence of the fast release component in the second Robo3 cKO example (A3).

(B) Quantifications of average and individual values of maximal presynaptic Ca^{2+} currents (left), basal presynaptic membrane capacitance (middle), and Ca^{2+} current density (bottom), in Robo3 cKO (red symbols) and control (black symbols) mice.

(C) Quantifications of average values of peak release rate (left), fast release time constant (middle), and the number of fast-released vesicles (right). When traces of cumulative release were best fitted with single-exponential functions (see A3 for an example), then the single-exponential time constant was plotted (C, middle; 8/20 synapses). Note the significant slowing of the fastest release time constant (middle), and the smaller number of FRP vesicles (right).

(D1) Example traces of presynaptic Ca^{2+} current (top) and of EPSCs (bottom) in response to 100 Hz trains of brief presynaptic depolarizations (1 ms to 28 mV). Data from paired recordings in a control mouse (left) and in a Robo3 cKO mouse (right) are shown. (D2) Plot of average EPSC amplitude during 100 Hz trains in control mice (n = 8; black symbols) and in Robo3 cKO mice (n = 8; red symbols).

(E1) Cumulative plot of EPSC amplitudes for the example EPSC traces shown in (D1). (E2) Average values for the readily releasable pool (RRP) size as obtained by back-extrapolation of the cumulative EPSC amplitude plots (left; see traces in E1 for examples), and for the release probability (right).

All recordings presented in this figure were obtained from P9–P12 old mice. The error bars represent SEM.

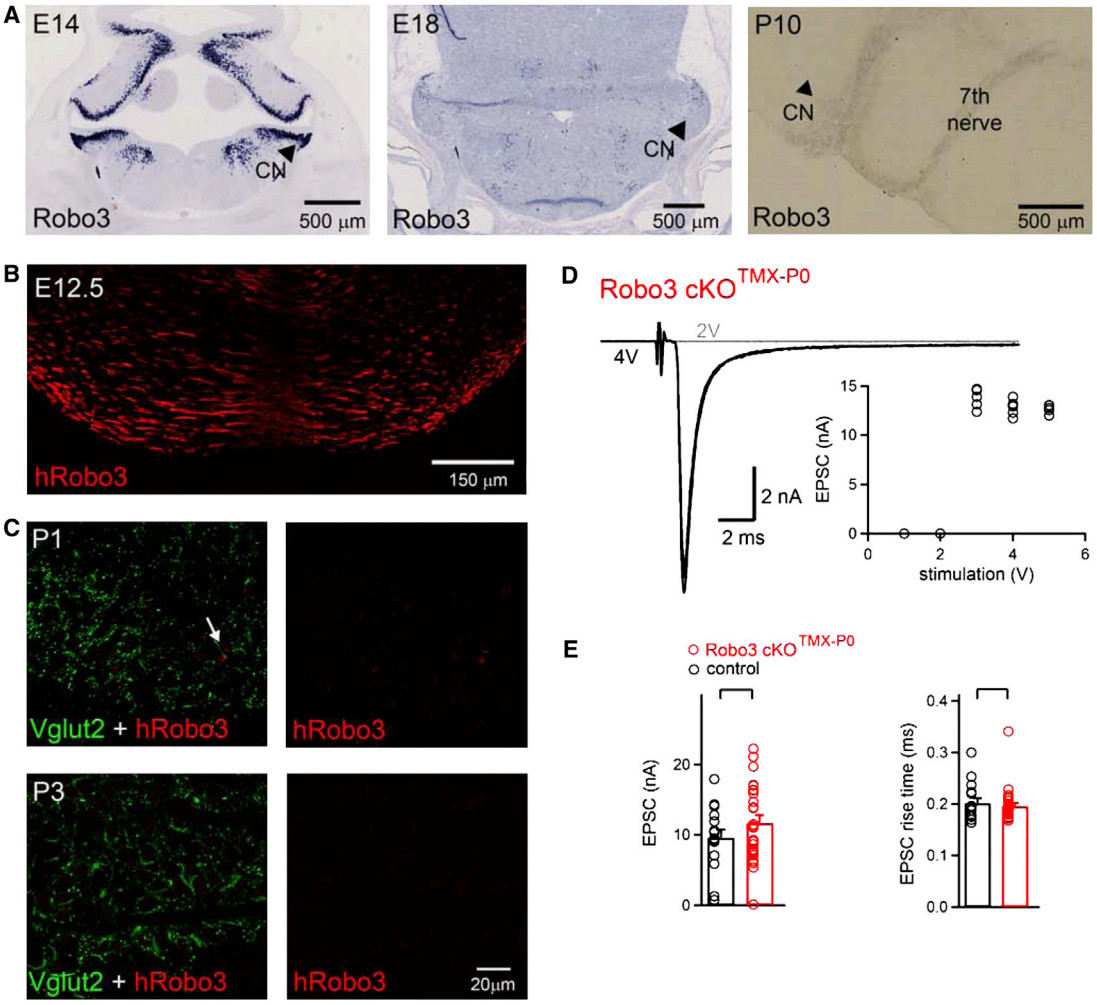

Figure 6. Robo3 Is Absent Early Postnatally, and Conditional Removal of Robo3 Early Postnatally Does Not Affect Synapse Function

(A) Results from in situ hybridization with a Robo3 probe at E14, E18 and at P10. Note the strong presence of Robo3 mRNA at E14 in the developing cochlear nucleus (CN). However, Robo3 expression is downregulated thereafter.

(B) Localization of the Robo3 protein in hindbrain axons at E12.5, as visualized by an anti-human Robo3 antibody.

(C) Immunohistochemistry in the MNTB area of a wild-type mouse at P1 (upper panel) and at P3 (lower panels). An anti-human Robo3 antibody (red channel) was used, together with an anti-VgluT2 antibody (green channel) as a marker for glutamatergic nerve terminals. Note the presence of small glutamatergic nerve terminals at P1 and of developing calyx nerve terminals at P3. Robo3 protein was absent except occasional stains (arrow); however, similar stains were occasionally observed in the Robo3 cKO mouse and therefore likely represent a nonspecific reaction (see Figure S1).

(D) Example EPSC traces recorded from a *CAGGS*$^{CreERTM/+}$, *Robo3*$^{lox/lox}$ mouse, injected at P0 with Tamoxifen, to induce the conditional recombination of the floxed Robo3 allele early postnatally. Note the large, single-fiber evoked EPSCs. The inset shows the corresponding plot of EPSC amplitude versus stimulation intensity.

(E) Plots of EPSC amplitude (*left panel*) and EPSC rise time (*right*), both for Robo3 cKO^{TMX-P0}, and for control mice. Note the unchanged EPSC amplitudes and rise times in Robo3 cKO^{TMX-P0} mice.

The recordings in (D) and (E) were made in P9– P12 mice. Error bars represent SEM. See also Figure S1.

axons at E12.5 (Figure 6B), we next attempted to localize Robo3 protein in developing calyces of Held early postnatally, at P1 and P3 (Figure 6C), and at P5 and P8 (see Figure S1 available online). Robo3 was undetectable in developing calyx of Held axons, despite occasional non-specific signals (Figure 6C, arrow); the latter persisted in Robo3 cKO mice (Figure S1). This data indicates that at the calyx of Held projection, Robo3 expression is developmentally downregulated before E18, similar as at other commissural projections (Marillat et al., 2004; Sabatier et al., 2004; Tamada et al., 2008). The absence of Robo3 argues against a direct role of this protein in synapse development.

To address a possible direct role of Robo3 in synapse development with an independent approach, we used a conditional KO approach with an inducible Cre mouse line, the *CAGGS::CreERTM* mouse line (Guo et al., 2002; Livet et al., 2007). *CAGGS*$^{CreERTM/+}$, *Robo3*$^{lox/lox}$ mice were injected at P0 with tamoxifen (referred to as Robo3 cKO^{TMX-P0} mice), in order to inactivate the floxed *Robo3* allele following axon midline

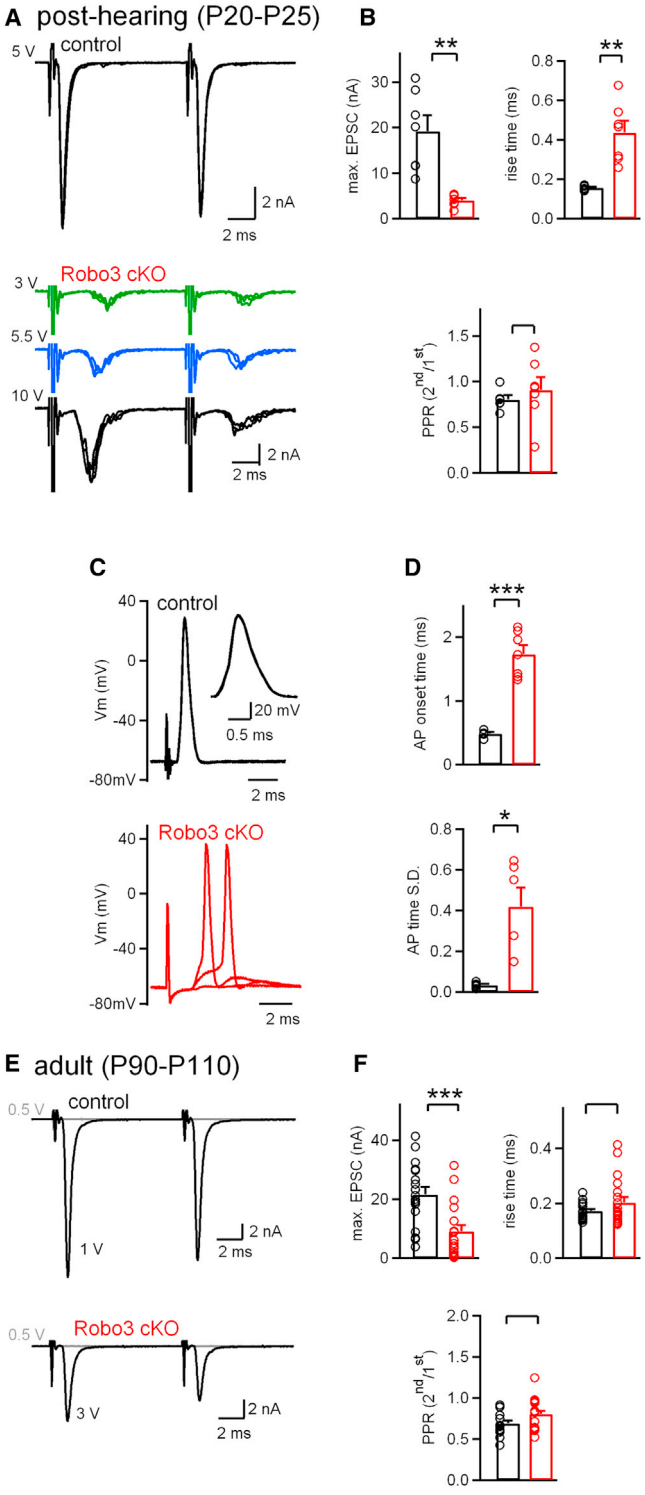

Figure 7. The Deficits in Synaptic Transmission in Robo3 cKO Mice Persist at Least up to the Young Hearing Age

(A) EPSC recordings from a control mouse (top panel) and from a Robo3 cKO mouse (bottom), at the indicated stimulation intensities.

(B) Bar graphs showing average and individual data points for maximal EPSC amplitude, 20%–80% EPSC rise time, and for paired-pulse ratio, both for control mice (black symbols), and for Robo3 cKO mice (red). Note the markedly smaller EPSC amplitude, and the significantly slower rise times ($p < 0.01$) also at this age range (P20–P25).

(C) Current clamp recording of EPSPs and EPSP-driven APs in MNTB principal neurons of a control mouse (top) and of a Robo3 cKO mouse (bottom). Repetition frequency, 0.1 Hz.

(D) Average values of AP onset times (top) and of the standard deviation of the AP onset time (bottom), in control (black symbols) and in Robo3 cKO mice (red symbols). Note the significantly longer, and more variable onset time of synaptically driven APs in the Robo3 cKO mice.

(E) EPSC recordings in slices from near - adult Robo3 cKO and control mice (P90–P110).

(F) Plots of average and individual EPSC data for adult (P90–P110) Robo3 cKO mice (red symbols) and their littermate control mice (black). Note the significantly ($p < 0.01$) smaller EPSC amplitude in adult Robo3 cKO mice compared to their littermate control mice.

The recordings presented in this figure were obtained from P20–P25 old mice (A–D), or from P90–P110 mice (E and F). The error bars represent SEM. See also Figure S2.

crossing, but before calyx of Held formation and - maturation. We then probed synaptic transmission at the calyx of Held at P9 to 12 (thus, 8–12 days postinjection) both in Robo3 cKO$^{TMX\text{-}P0}$ mice and in control mice (*CAGGS*$^{+/+}$, *Robo3*$^{lox/lox}$ mice injected with TMX at P0). Fiber stimulation evoked EPSCs in Robo3 cKO$^{TMX\text{-}P0}$ mice had an average amplitude of 11.7 ± 1.1 nA (n = 26), indistinguishable from EPSC amplitudes in control mice (9.6 ± 1.1 nA; n = 16; p = 0.2) (Figure 6E). Similarly, EPSC rise times were indistinguishable in Robo3 cKO$^{TMX\text{-}P0}$ mice (0.2 ± 0.006 ms, n = 26) as compared to control mice (0.2 ± 0.01 ms, n = 16; p = 0.58) (Figure 6E). Multiple innervation was essentially absent in Robo3 cKO$^{TMX\text{-}P0}$ and control mice (1 out of 26 and 1 out of 16 recordings, respectively). Therefore, the absence of detectable synaptic phenotypes upon postnatal inactivation of the floxed *Robo3* allele (Figures 6D and 6E), argues against a direct role of Robo3 in synapse development. We conclude that Robo3-dependent axon midline crossing conditions the later functional maturation of synaptic transmission at a commissural relay synapse (see Discussion).

The Deficits in Synaptic Transmission of Noncrossed Calyx Synapses Persist with Development

We showed that output synapses of non-crossed commissural axons in Robo3 cKO mice have a strong transmitter release deficit. Do these deficits merely represent a delay in the developmental acquisition of fast release properties, or do they persist with further development? To distinguish between these possibilities, we next investigated synaptic transmission in two older age groups of Robo3 cKO mice (Figure 7). In Robo3 cKO mice at an age group following hearing onset (P20– P25), we found strongly impaired synaptic transmission and multiple innervation (Figure 7A), similar as in the younger mice. The maximal EPSC amplitude was significantly smaller in Robo3 cKO mice (4.04 ± 1.31 nA) as compared to control mice (19.2 ± 3.51 nA; $p < 0.01$; Figure 7B). Several, up to three, presynaptic fibers mediated the EPSCs in Robo3 cKO mice, whereas the EPSCs in control mice were mediated by single fibers (Figure 7A). On the other hand, the paired-pulse ratio was not changed significantly between the genotypes (Figure 7B), different from the situation in the younger age group (Figures 3 and 5).

To assess how the reduced transmitter release in Robo3 cKO mice at P20– P25 affects the reliability and timing precision of EPSP - driven APs, we recorded EPSPs and postsynaptic APs under current-clamp (Figures 7C, 7D and S2). In control mice, we consistently observed very rapid initiation of postsynaptic APs with low timing variability, both with repeated stimuli at 0.1 Hz (Figure 7C) and during brief 100 Hz trains (Figure S2; Futai et al., 2001; Taschenberger and von Gersdorff, 2000). In contrast, in Robo3 cKO mice at P20– P25, single stimuli induced suprathreshold EPSPs in only 3 out of 7 recordings. Even when EPSPs were suprathreshold, APs were induced with a considerably greater timing variability in Robo3 cKO mice (Figures 7C, 7D, and S2). In conclusion, current clamp experiments in a post-hearing age group (P20– P25) indicate that the smaller EPSCs at calyx of Held synapses in Robo3 cKO mice can, in many cases, still generate a postsynaptic AP. However, the reduced transmitter release in these mice caused longer AP delays, and a decreased timing precision of postsynaptic APs. These differences were not caused by changes in the passive membrane properties nor in the intrinsic firing properties of MNTB cells, which were unchanged (Figure S2).

We also investigated Robo3 cKO mice at a near-adult age (P90– P110), to verify the possibility that some of the synaptic deficits might be remedied over much longer developmental periods. We found that EPSC amplitudes were still significantly smaller in Robo3 cKO mice (8.9 ± 2.2 nA; n = 19) as compared to control mice (21.5 ± 2.5 nA, n = 18; $p < 0.001$; Figures 7E and 7F). Multiple inputs were, however, seldomly observed in Robo3 cKO and control mice (2 out of n = 18 and 0 out of n = 19 recordings, respectively). Interestingly, the paired-pulse ratio, and the EPSC rise and decay times were unchanged (Figure 7F; $p > 0.05$). These findings suggest that the reduced release probability, and reduced release synchronicity found in young Robo3 cKO mice (Figures 3 and 5) recovered with further development, whereas the total synaptic strength remained significantly smaller. The latter finding might suggest that the size of the fast-releasable pool (FRP) remains reduced in Robo3 cKO mice up to adulthood.

A Downstream Inhibitory Synapse Is Not Affected in Robo3 cKO Mice

We have shown that genetic deletion of *Robo3*, a manipulation which forced the commissural calyx of Held axons to make synapses on the wrong (ipsilateral) brain side, strongly impairs the developmental maturation of presynaptic function. In order to investigate whether this effect of *Robo3* deletion is specific to mislocalized commissural synapses, or else, whether it represents a more general adaptive plasticity of the auditory network, we finally measured inhibitory postsynaptic currents (IPSCs) at the MNTB to LSO synapse.

Measuring IPSCs in LSO neurons at P10-P12 did not show obvious defects in inhibitory synaptic transmission (Figure 8). Several inhibitory synaptic inputs were detected upon gradual increase of the stimulation strength in both genotypes (Figure 8C; Kim and Kandler, 2003). The difference between successive stable amplitude levels in plots of IPSC amplitudes versus stimulus strength (Figures 8A and 8B) was taken as IPSC input amplitude. The IPSC input amplitudes varied largely within each cell, but were not different between Robo3 cKO and control mice on average (Figures 8C and 8D). Similarly, the rise time and decay time of the IPSCs were not different between the two genotypes (Figure 8E), indicating that there were no obvious changes in the synchronicity of transmitter release and the postsynaptic receptor kinetics, respectively. Therefore, the functional development of the MNTB to LSO synapse, a non-crossed inhibitory connection downstream of the commissural calyx of Held synapse, was unchanged in Robo3 cKO mice.

DISCUSSION

We have used conditional genetic removal of *Robo3* in the lower auditory system, coupled with patch-clamp electrophysiology and anatomical analyses, to investigate the functional consequences of a failure of commissural axon midline crossing. In Robo3 cKO mice, essentially all calyx of Held synapses were formed on the wrong, ipsilateral brain side. Calyces with their typical cup-shaped morphology initially formed, except for a slightly smaller size and a moderate deficit in the elimination of competing synaptic inputs. In contrast, the later functional maturation of transmitter release properties from ipsilateral calyces was strongly impaired. We observed that EPSCs had smaller amplitudes and slower rise times, indicating less transmitter release and reduced release synchronicity. Direct pre- and postsynaptic recordings showed that these defects were caused by a significantly smaller fast-releasable vesicle pool and by smaller and more variable presynaptic Ca^{2+} currents. Importantly, synaptic transmission deficits did not improve up to the age of young hearing mice, and only partially improved up to adulthood. These results indicate that localization of commissural output axons on the "correct" side of the brain conditions the later development of synapse function.

A Link between Axon Midline Crossing and the Functional Maturation of Commissural Output Synapses

The deficits in synapse function that we observed at a large commissural synapse in Robo3 cKO mice are most likely not caused by a direct role of Robo3 in synapse specification. Although Robo3 is a cell surface receptor and might potentially be involved in cell-cell contacts during the initial formation of calyces of Held or during later calyx maturation, Robo3 is not expressed at these later developmental times (Figure 6). The downregulation of Robo3 expression after E14, the time of axon midline crossing in this system (Howell et al., 2007), confirms previous findings at other commissural projections in spinal cord and hindbrain which indicate a selective expression of Robo3 at the time of axon midline crossing (Marillat et al., 2004; Sabatier et al., 2004; Tamada et al., 2008). In addition, our finding that temporally controlled, inducible inactivation of the *Robo3lox* allele at a time following axon midline crossing did not affect the development of synapse function (Figure 6), is further evidence against a direct role of Robo3 in calyx of Held formation, or in presynaptic maturation.

A more likely explanation for the marked presynaptic deficit in Robo3 cKO mice is that the early expression of *Robo3*, and/or midline crossing of commissural axons, has long-lasting consequences for the functional maturation of output synapses—thus,

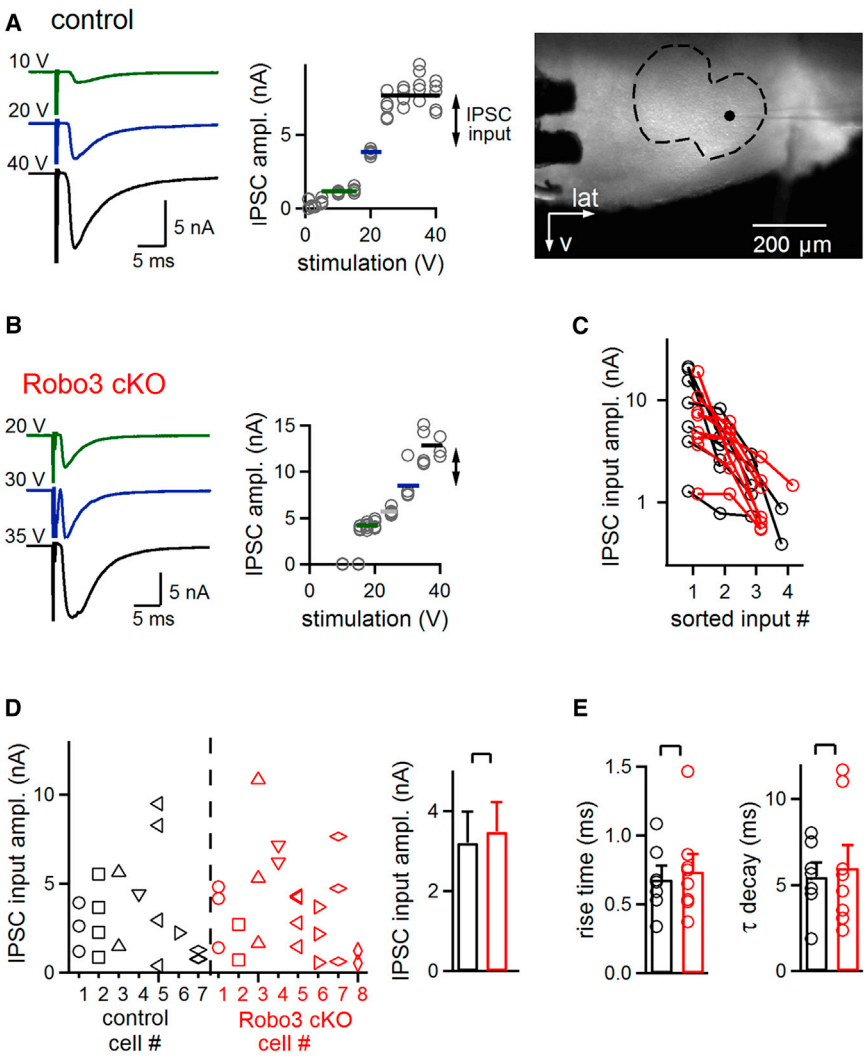

Figure 8. Inhibitory Synaptic Transmission in an Auditory Synapse Downstream of the MNTB Is Unchanged in Robo3 cKO Mice

(A) Fiber stimulation-evoked IPSCs (representative individual traces) recorded from an LSO neuron from a control mouse at the indicated stimulation intensities (left), and the corresponding plot of IPSC amplitudes versus stimulation intensity (right). The image on the right shows the placement of the stimulation electrode between the MNTB and the LSO. The outline of the LSO nucleus, and the position of the recording pipette are highlighted (dashed line, and black point, respectively).

(B) IPSC traces (left) and IPSC versus stimulation intensity (right), recorded in a LSO neuron from a Robo3 cKO mouse.

(C) Plot of the individual IPSC input amplitudes sorted according to size. Data points obtained in individual cells are connected by a line. Note the log scale of the y axis. The data for Robo3 cKO (red symbols) and control mice (black) largely overlap.

(D) Plot of individual IPSC input amplitude as a function of the cell number (left), and IPSC input amplitude averaged over all cells (right) in control mice (black symbols) and in Robo3 cKO mice (red).

(E) Average values of IPSC rise times (left) and of the time constants of the IPSC decay, both for control mice (black symbols) and for Robo3 cKO mice (red symbols).

All recordings presented in this Figure were obtained from P10–P12 old mice.

The error bars represent SEM.

axon midline crossing "conditions" synapse maturation. Although axons devoid of Robo3 still find their correct MNTB target neuron in terms of mediolateral localization (Figure 1), these axons may fail to express proteins that are normally upregulated after midline crossing, such as Robo1 and Robo2 or plexin-A1 (Jaworski et al., 2010; Long et al., 2004; Nawabi et al., 2010). Axons that failed to cross the midline might also continue to express proteins that are normally downregulated following midline crossing, such as deleted in colorectal cancer (DCC) (Howell et al., 2007; see Chédotal, 2011 for a review). Interestingly, DCC has been shown to associate with the protein synthesis machinery and to regulate protein translation in axons (Brittis et al., 2002; Tcherkezian et al., 2010). Therefore, a dysregulation of axonal protein synthesis following a failure of axon midline crossing could lead to expression changes of presynaptic proteins, and/or trophic factors relevant for the maturation of synapse function. It was shown recently that the absence of RIM1 and RIM2 proteins at the calyx of Held results in a marked reduction of presynaptic Ca^{2+} currents, and a smaller fast-releasable vesicle pool (Han et al., 2011). The variable Ca^{2+} current density and smaller vesicle pools observed here in Robo3 cKO mice are reminiscent of the RIM1/2 KO phenotype. It is possible that the decreased presynaptic function of calyx synapses of Robo3 cKO mice is the consequence of reduced levels of RIM protein, or of other proteins involved in the functional organization of active zones (Schoch and Gundelfinger, 2006). It is noteworthy that while functional maturation of Ca^{2+} channel-release coupling is well documented at the calyx synapse (Chuhma et al., 2001; Fedchyshyn and Wang, 2005; Taschenberger and von Gersdorff, 2000), the underlying changes in presynaptic protein expression and/or post-translational changes of presynaptic proteins are largely unknown (but see Yang et al., 2010).

We observed that the functional maturation of most calyces of Held was defective in Robo3 cKO mice, while the initial formation of the typical calyx structure, despite a moderate synapse elimination deficit, was largely unchanged. Therefore, it seems that a program of morphological growth of calyces was not strongly affected in Robo3 cKO mice. It has been shown that unilateral inner ear removal and the ensuing degeneration of the cochlear nucleus and denervation of the contralateral MNTB, leads to sprouting of GBC axons which can form ipsilateral calyces of quite typical morphology (Hsieh et al., 2007; Kitzes et al., 1995). In this denervation paradigm, a program of morphological

calyx formation also seems to take place readily. Of note, denervation-induced ipsilateral calyces arise from axons that have already successfully crossed the midline. Therefore, ipsilateral calyces formed after denervation might show normal functional maturation, a possibility that should be tested in future work.

The trophic factors and signaling molecules that drive the morphological development of the highly specialized calyx-type synapses, which are found on several levels of the lower auditory system (Grothe et al., 2010), are just beginning to be investigated (Nakamura and Cramer, 2011). Studies at the *Drosophila* neuromuscular synapse have shown that BMPs (bone morphogenetic proteins) function as a retrograde messenger involved in the growth of the motor nerve terminal (Aberle et al., 2002; Marqués et al., 2002). We have recently obtained evidence for a role of BMP signaling in calyx growth and competing synapse elimination, as well as in the subsequent functional maturation of transmitter release (Xiao et al., 2013). It has also been found that brain-derived neurotrophic factor (BDNF) is necessary for the axonal translation of SMAD proteins, a signaling component downstream of BMP signaling (Ji and Jaffrey, 2012). Together with the present findings on Robo3 cKO mice, this suggests the interesting possibility that a dysregulation of axonal protein synthesis in non-crossed axons, as hypothesized above, could lead to impaired trophic signaling necessary for the later functional maturation of calyx-type synapses.

Conditioned Maturation of Commissural Output Synapses and Circuit Function

We found that most deficits in synapse function in Robo3 cKO mice persist at least up to young hearing mice (P20– P25), and the decreased synaptic strength persisted up to adulthood in Robo3 cKO mice (Figure 7). This suggests that mislocalized calyx synapses do not merely experience a slight delay of synapse maturation in Robo3 cKO mice. Rather, it seems that the function of mislocalized calyces of Held is suppressed as a consequence of an irreversible change during early development, following absence of axon midline crossing (see above). Noncrossed calyx of Held axons would cause the downstream inhibitory synapse, the MNTB to LSO synapse, to be activated on the wrong brain side, and thereby cause a distortion of the computation of sound source localization performed in these auditory circuits. It might therefore be advantageous to not permit mislocalized commissural synapses to develop strong transmitter release. Alternatively, the circuit could react by downregulating the development of the synapses downstream of the mislocalized commissural synapse—in this case, the inhibitory output synapse of MNTB neuron projections (Figure 1). This, however, was not observed (Figure 8). This suggests that we have uncovered a mechanism of conditioned maturation of commissural output synapses, which takes place in axons that normally express Robo3 early-on. This mechanism contrasts with a more widespread adaptive or compensatory plasticity, which could also act on other synapses of the same circuit.

Consequences for Human Disease

In humans, mutations in *ROBO3* cause horizontal gaze palsy (absence of conjugate eye movement) with progressive scoliosis (HGPPS syndrome) (Jen et al., 2004). HGPPS patients have a general hypoplasia of the hindbrain and a disruption of hindbrain and other commissures (Amoiridis et al., 2006; Haller et al., 2008; Jen et al., 2004). In the patients, crossed and uncrossed stapedius reflex could not be elicited, and wave III of the auditory brainstem response (ABR), which is thought to be caused by the electrical activity of neurons located in the superior olive, was delayed (Amoiridis et al., 2006). A distorted ABR was also found in the Robo3 cKO mice (Renier et al., 2010). Although the performance of HGPPS patients in localizing sound source has not been tested, no obvious major deficits have been reported, and HGPPS patients do not have overt cognitive deficits or noticeable motor or sensory-motor deficits (Haller et al., 2008). We speculate that the conditioned maturation of commissural axon output synapses might limit the expected detrimental effects of uncrossed commissural axons on the cognitive and sensory abilities of HGPPS patients. Therefore, the conditioned functional maturation of a commissural output synapse uncovered here might contribute to compensatory mechanisms that help HGPPS patients to develop near-normal degrees of sensory and motor functions, despite the fact that major commissural systems are un-crossed.

EXPERIMENTAL PROCEDURES

Conditional *Robo3* Knockout Mice Specific for the Auditory Brainstem

We used the *Krox20::Cre* mouse line (Voiculescu et al., 2000; gift of Patrick Charnay, Paris, France), which drives *Cre* expression in the lower auditory brainstem (Han et al., 2011; Maricich et al., 2009), to recombine the floxed *Robo3* allele and to suppress axon midline crossing in the calyx of Held projection (Renier et al., 2010). Heterozygous $Krox20^{Cre/+}$ mice were crossed with $Robo3^{lox/lox}$ mice (Renier et al., 2010); the early expression onset of Cre-recombinase under the *Krox20* promoter (~E10; Voiculescu et al., 2000) ensured that the floxed *Robo3* allele was recombined early enough to prevent axon midline crossing. Additional breeding methods, and methods regarding the *CAGGS::CreERTM* approach are given in Supplemental Experimental Procedures.

Electrophysiology and Data Analysis

Transverse 200 μm thick slices of the brainstem containing the MNTB and LSO nuclei were made according to standard procedures with a LEICA VT1000S vibratome, using Robo3 cKO and control mice of three different age groups: P9–P12, P20–P25, and P90–P110. Protocols of mouse handling and animal experimentation were approved by the Veterinary office of the Canton of Vaud, Switzerland (authorization # 2063). The extracellular recording solutions were bicarbonate-based Ringer solutions containing 2 mM $CaCl_2$ and 1 mM $MgCl_2$ (see Supplemental Experimental Procedures for detailed composition). For the recordings of fiber stimulation-evoked EPSCs (Figures 2 and 6), bicuculline (10 μM) and strychnine (2 μM) were added to the extracellular solution. For recordings of IPSCs in LSO principal neurons (Figure 8), NBQX (10 μM) was added. For paired recordings (Figure 5), tetraethylammonium chloride (TEA, 10 mM), tetrodotoxin (TTX, 1 μM), D-AP5 (50 μM), γ-D-glutamylglycine (γ-DGG, 2 mM), cyclothiazide (CTZ, 100 μM), bicuculline (10 μM), and strychnine (2 μM) were added to the extracellular solution. We used four different pipette solutions: (1) a Cs-gluconate based solution with 5 mM EGTA, for recording of MNTB neurons in the voltage clamp mode (Figures 2, 3, 5, 6, and 7); (2) a Cs-gluconate based solution with 0.1 mM EGTA for presynaptic recordings in paired recordings (Figure 5); (3) a K-gluconate based solution with 5 mM EGTA for recording MNTB neurons in current-clamp mode (Figures 7C, 7D, and S1); (4) a CsCl-based solution with high $[Cl^-]_i$ (150 mM) and 5 mM EGTA for recording IPSCs in LSO neurons (Figure 8). The detailed compositions of all pipette solutions, as well as further details concerning patch pipette

resistances, series resistance (R_s) during recording and off-line R_s compensation of EPSC and IPSC traces, are given in Supplemental Experimental Procedures.

Data analysis was performed using the IgorPro software. Rates of transmitter release were determined by EPSC deconvolution analysis using routines written in IgorPro by Neher and Sakaba (2001). Data are reported as average ± SEM values, and statistical significance was evaluated using unpaired, two-tailed t test with Welch's correction (Prism software). Statistical significance was accepted at $p < 0.05$. Asterisks above brackets in data bar graphs indicate the level of statistical significance (*$p < 0.05$; **$p < 0.01$; and ***$p < 0.001$). A bracket without symbol indicates $p > 0.05$ (not significant).

The methods for immunohistochemistry and in situ hybridization, as well as DiI tracing and acoustic labeling experiments, are given in Supplemental Experimental Procedures.

SUPPLEMENTAL INFORMATION

Supplemental Information includes two figures and Supplemental Experimental Procedures and can be found with this article online at http://dx.doi.org/10.1016/j.neuron.2013.04.006.

ACKNOWLEDGMENTS

We thank Jessica Dupasquier, Coraly Pernet, Heather Murray, and Nicolas Rama for expert technical assistance, Enida Gjoni for help with LSO recordings, and Jean-Pierre Hardelin for critical comments on the manuscript. This research was supported by a Marie Curie post-doctoral fellowship (IEF-235223-Calyx-MMFF to N.M.), the Swiss National Science Foundation (SNF; Sinergia grant CRSI33_127440/1 to R.S.), the National Center of Competence in Research (NCCR) of the SNF "Synaptic Bases of Mental Disease," the Fondation pour recherche médicale (FRM; to A.C.), the Association Française contre les Myopathies (AFM, ASS-SUB06-00123; to A.C.), the Labex lifesenses (to A.C.), and the Agence Nationale de la Recherche (ANR-2011 BSV 40091; to A.C.)

Accepted: April 4, 2013
Published: May 9, 2013

REFERENCES

Aberle, H., Haghighi, A.P., Fetter, R.D., McCabe, B.D., Magalhães, T.R., and Goodman, C.S. (2002). wishful thinking encodes a BMP type II receptor that regulates synaptic growth in *Drosophila*. Neuron *33*, 545–558.

Amoiridis, G., Tzagournissakis, M., Christodoulou, P., Karampekios, S., Latsoudis, H., Panou, T., Simos, P., and Plaitakis, A. (2006). Patients with horizontal gaze palsy and progressive scoliosis due to ROBO3 E319K mutation have both uncrossed and crossed central nervous system pathways and perform normally on neuropsychological testing. J. Neurol. Neurosurg. Psychiatry *77*, 1047–1053.

Bergsman, J.B., De Camilli, P., and McCormick, D.A. (2004). Multiple large inputs to principal cells in the mouse medial nucleus of the trapezoid body. J. Neurophysiol. *92*, 545–552.

Borst, J.G., and Soria van Hoeve, J. (2012). The calyx of held synapse: from model synapse to auditory relay. Annu. Rev. Physiol. *74*, 199–224.

Brittis, P.A., Lu, Q., and Flanagan, J.G. (2002). Axonal protein synthesis provides a mechanism for localized regulation at an intermediate target. Cell *110*, 223–235.

Brose, K., Bland, K.S., Wang, K.H., Arnott, D., Henzel, W., Goodman, C.S., Tessier-Lavigne, M., and Kidd, T. (1999). Slit proteins bind Robo receptors and have an evolutionarily conserved role in repulsive axon guidance. Cell *96*, 795–806.

Cant, N.B., and Benson, C.G. (2003). Parallel auditory pathways: projection patterns of the different neuronal populations in the dorsal and ventral cochlear nuclei. Brain Res. Bull. *60*, 457–474.

Chédotal, A. (2011). Further tales of the midline. Curr. Opin. Neurobiol. *21*, 68–75.

Chuhma, N., Koyano, K., and Ohmori, H. (2001). Synchronisation of neurotransmitter release during postnatal development in a calyceal presynaptic terminal of rat. J. Physiol. *530*, 93–104.

Dickson, B.J. (2002). Molecular mechanisms of axon guidance. Science *298*, 1959–1964.

Ehret, G. (1976). Development of absolute auditory thresholds in the house mouse (Mus musculus). J. Am. Audiol. Soc. *1*, 179–184.

Farago, A.F., Awatramani, R.B., and Dymecki, S.M. (2006). Assembly of the brainstem cochlear nuclear complex is revealed by intersectional and subtractive genetic fate maps. Neuron *50*, 205–218.

Fazeli, A., Dickinson, S.L., Hermiston, M.L., Tighe, R.V., Steen, R.G., Small, C.G., Stoeckli, E.T., Keino-Masu, K., Masu, M., Rayburn, H., et al. (1997). Phenotype of mice lacking functional Deleted in colorectal cancer (Dcc) gene. Nature *386*, 796–804.

Fedchyshyn, M.J., and Wang, L.-Y. (2005). Developmental transformation of the release modality at the calyx of Held synapse. J. Neurosci. *25*, 4131–4140.

Friauf, E. (1992). Tonotopic order in the adult and developing auditory system of the rat as shown by c-fos immunocytochemistry. Eur. J. Neurosci. *4*, 798–812.

Futai, K., Okada, M., Matsuyama, K., and Takahashi, T. (2001). High-fidelity transmission acquired via a developmental decrease in NMDA receptor expression at an auditory synapse. J. Neurosci. *21*, 3342–3349.

Grothe, B., Pecka, M., and McAlpine, D. (2010). Mechanisms of sound localization in mammals. Physiol. Rev. *90*, 983–1012.

Guo, C., Yang, W., and Lobe, C.G. (2002). A Cre recombinase transgene with mosaic, widespread tamoxifen-inducible action. Genesis *32*, 8–18.

Habets, R.L.P., and Borst, J.G.G. (2005). Post-tetanic potentiation in the rat calyx of Held synapse. J. Physiol. *564*, 173–187.

Haller, S., Wetzel, S.G., and Lütschg, J. (2008). Functional MRI, DTI and neurophysiology in horizontal gaze palsy with progressive scoliosis. Neuroradiology *50*, 453–459.

Han, Y., Kaeser, P.S., Südhof, T.C., and Schneggenburger, R. (2011). RIM determines Ca^{2+} channel density and vesicle docking at the presynaptic active zone. Neuron *69*, 304–316.

Hoffpauir, B.K., Grimes, J.L., Mathers, P.H., and Spirou, G.A. (2006). Synaptogenesis of the calyx of Held: rapid onset of function and one-to-one morphological innervation. J. Neurosci. *26*, 5511–5523.

Hoffpauir, B.K., Kolson, D.R., Mathers, P.H., and Spirou, G.A. (2010). Maturation of synaptic partners: functional phenotype and synaptic organization tuned in synchrony. J. Physiol. *588*, 4365–4385.

Howell, D.M., Morgan, W.J., Jarjour, A.A., Spirou, G.A., Berrebi, A.S., Kennedy, T.E., and Mathers, P.H. (2007). Molecular guidance cues necessary for axon pathfinding from the ventral cochlear nucleus. J. Comp. Neurol. *504*, 533–549.

Hsieh, C.Y., Hong, C.T., and Cramer, K.S. (2007). Deletion of EphA4 enhances deafferentation-induced ipsilateral sprouting in auditory brainstem projections. J. Comp. Neurol. *504*, 508–518.

Iwasaki, S., Momiyama, A., Uchitel, O.D., and Takahashi, T. (2000). Developmental changes in calcium channel types mediating central synaptic transmission. J. Neurosci. *20*, 59–65.

Jaworski, A., Long, H., and Tessier-Lavigne, M. (2010). Collaborative and specialized functions of Robo1 and Robo2 in spinal commissural axon guidance. J. Neurosci. *30*, 9445–9453.

Jen, J.C., Chan, W.M., Bosley, T.M., Wan, J., Carr, J.R., Rüb, U., Shattuck, D., Salamon, G., Kudo, L.C., Ou, J., et al. (2004). Mutations in a human ROBO gene disrupt hindbrain axon pathway crossing and morphogenesis. Science *304*, 1509–1513.

Ji, S.J., and Jaffrey, S.R. (2012). Intra-axonal translation of SMAD1/5/8 mediates retrograde regulation of trigeminal ganglia subtype specification. Neuron *74*, 95–107.

Kidd, T., Bland, K.S., and Goodman, C.S. (1999). Slit is the midline repellent for the robo receptor in Drosophila. Cell *96*, 785–794.

Kim, G., and Kandler, K. (2003). Elimination and strengthening of glycinergic/GABAergic connections during tonotopic map formation. Nat. Neurosci. *6*, 282–290.

Kitzes, L.M., Kageyama, G.H., Semple, M.N., and Kil, J. (1995). Development of ectopic projections from the ventral cochlear nucleus to the superior olivary complex induced by neonatal ablation of the contralateral cochlea. J. Comp. Neurol. *353*, 341–363.

Korogod, N., Lou, X., and Schneggenburger, R. (2005). Presynaptic Ca^{2+} requirements and developmental regulation of posttetanic potentiation at the calyx of Held. J. Neurosci. *25*, 5127–5137.

Livet, J., Weissman, T.A., Kang, H., Draft, R.W., Lu, J., Bennis, R.A., Sanes, J.R., and Lichtman, J.W. (2007). Transgenic strategies for combinatorial expression of fluorescent proteins in the nervous system. Nature *450*, 56–62.

Long, H., Sabatier, C., Ma, L., Plump, A., Yuan, W., Ornitz, D.M., Tamada, A., Murakami, F., Goodman, C.S., and Tessier-Lavigne, M. (2004). Conserved roles for Slit and Robo proteins in midline commissural axon guidance. Neuron *42*, 213–223.

Maricich, S.M., Xia, A., Mathes, E.L., Wang, V.Y., Oghalai, J.S., Fritzsch, B., and Zoghbi, H.Y. (2009). Atoh1-lineal neurons are required for hearing and for the survival of neurons in the spiral ganglion and brainstem accessory auditory nuclei. J. Neurosci. *29*, 11123–11133.

Marillat, V., Sabatier, C., Failli, V., Matsunaga, E., Sotelo, C., Tessier-Lavigne, M., and Chédotal, A. (2004). The slit receptor Rig-1/Robo3 controls midline crossing by hindbrain precerebellar neurons and axons. Neuron *43*, 69–79.

Marqués, G., Bao, H., Haerry, T.E., Shimell, M.J., Duchek, P., Zhang, B., and O'Connor, M.B. (2002). The Drosophila BMP type II receptor Wishful Thinking regulates neuromuscular synapse morphology and function. Neuron *33*, 529–543.

Miko, I.J., Nakamura, P.A., Henkemeyer, M., and Cramer, K.S. (2007). Auditory brainstem neural activation patterns are altered in EphA4- and ephrin-B2-deficient mice. J. Comp. Neurol. *505*, 669–681.

Nakamura, P.A., and Cramer, K.S. (2011). Formation and maturation of the calyx of Held. Hear. Res. *276*, 70–78.

Nawabi, H., Briançon-Marjollet, A., Clark, C., Sanyas, I., Takamatsu, H., Okuno, T., Kumanogoh, A., Bozon, M., Takeshima, K., Yoshida, Y., et al. (2010). A midline switch of receptor processing regulates commissural axon guidance in vertebrates. Genes Dev. *24*, 396–410.

Neher, E., and Sakaba, T. (2001). Combining deconvolution and noise analysis for the estimation of transmitter release rates at the calyx of held. J. Neurosci. *21*, 444–461.

Renier, N., Schonewille, M., Giraudet, F., Badura, A., Tessier-Lavigne, M., Avan, P., De Zeeuw, C.I., and Chédotal, A. (2010). Genetic dissection of the function of hindbrain axonal commissures. PLoS Biol. *8*, e1000325.

Rodríguez-Contreras, A., van Hoeve, J.S., Habets, R.L., Locher, H., and Borst, J.G. (2008). Dynamic development of the calyx of Held synapse. Proc. Natl. Acad. Sci. USA *105*, 5603–5608.

Sabatier, C., Plump, A.S., Ma, Le, Brose, K., Tamada, A., Murakami, F., Lee, E.Y., and Tessier-Lavigne, M. (2004). The divergent Robo family protein rig-1/Robo3 is a negative regulator of slit responsiveness required for midline crossing by commissural axons. Cell *117*, 157–169.

Sakaba, T. (2006). Roles of the fast-releasing and the slowly releasing vesicles in synaptic transmission at the calyx of held. J. Neurosci. *26*, 5863–5871.

Sakaba, T., and Neher, E. (2001). Calmodulin mediates rapid recruitment of fast-releasing synaptic vesicles at a calyx-type synapse. Neuron *32*, 1119–1131.

Sanes, J.R., and Yamagata, M. (2009). Many paths to synaptic specificity. Annu. Rev. Cell Dev. Biol. *25*, 161–195.

Schneggenburger, R., Meyer, A.C., and Neher, E. (1999). Released fraction and total size of a pool of immediately available transmitter quanta at a calyx synapse. Neuron *23*, 399–409.

Schoch, S., and Gundelfinger, E.D. (2006). Molecular organization of the presynaptic active zone. Cell Tissue Res. *326*, 379–391.

Serafini, T., Colamarino, S.A., Leonardo, E.D., Wang, H., Beddington, R., Skarnes, W.C., and Tessier-Lavigne, M. (1996). Netrin-1 is required for commissural axon guidance in the developing vertebrate nervous system. Cell *87*, 1001–1014.

Shen, K., and Scheiffele, P. (2010). Genetics and cell biology of building specific synaptic connectivity. Annu. Rev. Neurosci. *33*, 473–507.

Sherman, S.M., and Guillery, R.W. (1998). On the actions that one nerve cell can have on another: distinguishing "drivers" from "modulators". Proc. Natl. Acad. Sci. USA *95*, 7121–7126.

Tamada, A., Kumada, T., Zhu, Y., Matsumoto, T., Hatanaka, Y., Muguruma, K., Chen, Z., Tanabe, Y., Torigoe, M., Yamauchi, K., et al. (2008). Crucial roles of Robo proteins in midline crossing of cerebellofugal axons and lack of their up-regulation after midline crossing. Neural Dev. *3*, 29.

Taschenberger, H., and von Gersdorff, H. (2000). Fine-tuning an auditory synapse for speed and fidelity: developmental changes in presynaptic waveform, EPSC kinetics, and synaptic plasticity. J. Neurosci. *20*, 9162–9173.

Tcherkezian, J., Brittis, P.A., Thomas, F., Roux, P.P., and Flanagan, J.G. (2010). Transmembrane receptor DCC associates with protein synthesis machinery and regulates translation. Cell *141*, 632–644.

Voiculescu, O., Charnay, P., and Schneider-Maunoury, S. (2000). Expression pattern of a Krox-20/Cre knock-in allele in the developing hindbrain, bones, and peripheral nervous system. Genesis *26*, 123–126.

Walmsley, B., Alvarez, F.J., and Fyffe, R.E.W. (1998). Diversity of structure and function at mammalian central synapses. Trends Neurosci. *21*, 81–88.

Xiao, L., Michalski, N., Kronander, E., Gjoni, E., Genoud, C., Knott, G., and Schneggenburger, R. (2013). BMP signaling specifies the development of a large and fast CNS synapse. Nat. Neurosci. http://dx.doi.org/10.1038/nn.3414

Yang, Y.M., Fedchyshyn, M.J., Grande, G., Aitoubah, J., Tsang, C.W., Xie, H., Ackerley, C.A., Trimble, W.S., and Wang, L.Y. (2010). Septins regulate developmental switching from microdomain to nanodomain coupling of $Ca(^{2+})$ influx to neurotransmitter release at a central synapse. Neuron *67*, 100–115.

Ypsilanti, A.R., Zagar, Y., and Chédotal, A. (2010). Moving away from the midline: new developments for Slit and Robo. Development *137*, 1939–1952.